Geodesic voting methods: overview, extensions, and application to blood vessel segmentation

Youssef Rouchdy and Laurent D. Cohen
CEREMADE, Université Paris Dauphine, 75775 PARIS CEDEX 16 - FRANCE

Abstract

This paper presents new methods to segment thin tree structures, which are, for example present in microglia extensions and cardiac or neuronal blood vessels. Many authors have used minimal cost paths, or geodesics relative to a local weighting potential P, to find a vessel pathway between two end points. We utilize a set of such geodesic paths to find a tubular tree structure by seeking minimal interaction. Recently, we introduced a set of methods called geodesic voting. In this article we review all these methods and present some extensions. We also adapt these methods to the segmentation of complex tree structures in a noisy medium and apply them to the segmentation of blood vessels in 2D and 3D.

Keywords: Geodesic Voting, Fast Marching, Level Set, Minimal Paths, Tree Structure Segmentation.

1. Introduction

In this paper we present novel methods for the segmentation of tree structures. These methods are based on minimal paths and can be applied to extract numerous structures such as microglia extensions, neurovascular structures, blood vessels, and pulmonary trees. There are many studies dedicated

to the extraction of vascular or airway trees. For a review of such methods see [1, 2, 3, 4, 5, 6]. Among the approaches used to segment such tree structures, we consider three models, classified according to their method for extracting the tubular aspect of the tree: centerline based models; surface models; and 4D curve models. The first category focuses on directly extracting the centerlines of the tubular tree [7, 8]. After extracting the centerlines a second process can be used to segment the lumen of the tree, see [9]. The second category directly extracts the surface of the vessel. These approaches includes explicit and implicit surface models. The former use a parametric representation of the tubular structure [10]. These models are not adapted to the segmentation of complex tree structures, while the latter implicit methods can evolve the surface through complex shape changes including changes in topology [11, 12]. However, initialization must be performed carefully to obtain an accurate segmentation.

Minimal path techniques are extensively used for centerline extraction of tubular tree structures. These approaches are robust to the presence of local perturbations due to stenosed branches of the tree or imaging artifacts where the local image information might be insufficient to guide the shape evolution process. Several minimal path techniques have been proposed to deal with this problem [13, 14, 15, 16]. These techniques involve designing a metric from the image in such way that the tubular structures correspond to geodesic paths according to this metric [17]. Solving the problem from the practical point of view consists of a front propagation from a source point within a vessel, which moves faster along the branches of the vascular tree. These methods require the user to supply a starting point (propagation

source) and end points. Each end point results in an extracted minimal path back to the source point. The points located along this minimal path are very likely to be located on the vessel of interest. A small amount of work has been devoted to reduce the need for user intervention of the user in the segmentation of tree structure to the initialization of the propagation from a single point. The authors of [18] defined a stopping criterion based on a "medialness" measure; the propagation is stopped when "medialness" drops below a given threshold. This method might suffer from the same problem as region growing since the medialness measure might drop below the given threshold in the presence of lesions or other local image artifacts. In [14], the authors proposed stopping the propagation when the geodesic distance reaches a certain value. However, this method is limited to the segmentation of a single vessel and the definition of the threshold of the geodesic distance is not straightforward. The authors of [19] proposed stopping the propagation according to a criterion based on certain geometric properties of the region covered by the front. In [15], assuming the total length of the tree structure to be visited is roughly given, the stopping criterion is based on the Euclidean length of the minimal path.

In this paper, we present new methods to extract tree structures without using any *a priori* information and using only a single user provided point on the tree structure. The methods are generic, they can be used to extract any type of tree structure in 2D as well as in 3D. These methods were presented separately in conferences [20, 21, 22, 23]. Here, we provide an overview of all these methods and propose extensions. The approach is based on a completely new concept, namely, Geodesic Voting. It consists of computing

geodesics from a given source point to a set of end points scattered throughout the image. The target structure corresponds to image points with a high geodesic density. The geodesic density is defined at each pixel of the image as the number of geodesics that pass over this pixel. Since the potential exhibits low values along the tree structure, geodesics will preferably migrate toward this structure and thereby yield a high geodesic density. We introduce different approaches to segment complex tree structures in noisy media environments and apply them to segment blood vessels in medical images.

In Section 2 we introduce the geodesic voting approach. In Section 3, we propose a variety of possible ways to obtain both the centerline and the boundary of the vascular tree. In Section 4 we evaluate the method on 2D retinal images.

2. Background

2.1. Minimal paths

In the context of image segmentation Cohen and Kimmel proposed, in [17], a deformable model to extract contours between two points given by the user. The model is formulated as finding a geodesic for a weighted distance:

$$\min_{y} \int_0^L (w + P(y(s)))\mathrm{d}s, \tag{1}$$

the minimum is considered over all curves $y(s)$ traced on the image domain Ω that link the two end points, that is, $y(0) = x_0$ and $y(L) = x_1$. The constant w imposes regularity on the curve. $P > 0$ is a potential cost function computed from the image, it takes lower values near the edges or the features.

For instance $P(y(s)) = I(y(s))$ leads to darker lines while $P(y(s)) = g(||\nabla I||)$ leads to edges, where I is the image and g is a decreasing positive function.

To compute the solution associated to the source x_0 of this problem, [17] proposed a Hamiltonian approach: Find the geodesic weighted distance U that solves the Eikonal equation: $||\nabla \mathrm{U}(x)|| = w + P(x),\ \forall x \in \Omega$. The ray y is subsequently computed by back-propagation from the end point x_1 by solving the Ordinary Differential Equation (ODE):

$$y'(s) = -\nabla \mathrm{U}(y). \tag{2}$$

The idea behind the Fast Marching algorithm is to propagate the wave in only one direction, starting with the smaller values of the action map U and progressing to the larger values using the upwind property of the scheme. Therefore, the Fast Marching method permits to solve the Eikonal in complexity $O(n \log(n))$, for details see [17].

2.2. Geodesic voting for the segmentation of tree structures

We have introduced in [20] a new concept to segment a tree structure from only one point given by the user in the tree structure. This method consists in computing the geodesic density from a set of geodesics extracted from the image. Assume you are looking for a tree structure for which a potential cost function has been defined as above and has lower values on this tree structure. First we provide a starting point x_0 roughly at the root of the tree structure and we propagate a front in the whole image with the Fast Marching method, obtaining the minimal action U. Then assume you consider an end point anywhere in the image. Backtracking the minimal path

from the end point you will reach the tree structure somewhere and stay on it till the start point is reached. So a part of the minimal path lies on some branches of the tree structure. The idea of this approach is to consider a large number of end points $\{x_k\}_{k=1}^N$ on the image domain, and analyze the set of minimal paths y_k obtained. For this we consider a voting scheme along the centerlines. When backtracking each path, you add 1 to each pixel you pass over. At the end of this process, pixels on the tree structure will have a high vote since many paths have to pass over it. On the contrary, pixels in the background will generally have a low vote since very few paths will pass over them. The result of this voting scheme is what we can call the geodesic density. This means at each pixel the density of geodesics that pass over this pixel. The tree structure corresponds to the points with high geodesic density.

The set of end points for which you consider the geodesics can be defined through different choices. This could be all pixels over the image domain, random points, scattered points according to some criterion, or simply the set of points on the boundary of the image domain. We define the voting score or the geodesic density at each pixel p of the image by

$$\mu(p) = \sum_{k=1}^{N} \delta_p(y_k) \tag{3}$$

where the function $\delta_p(y)$ returns 1 if the path y crosses the pixel p, else 0. Once the geodesic voting is made, the tree structure is obtained by a simple thresholding of the geodesic density μ. As shown in [22] and Figure 1, the contrast between the background and the tree is large and the threshold can be chosen easily.

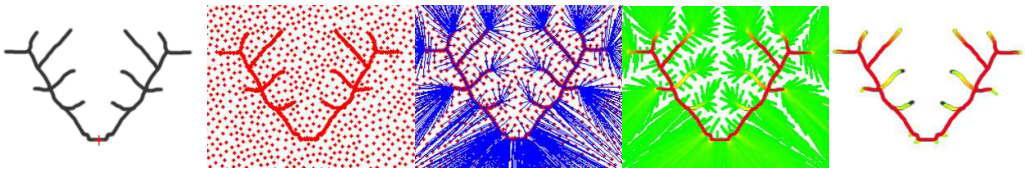

Figure 1: Geodesic Voting method. From the left to the right: the first panel shows the synthetic tree, the red cross represents the root of the tree; the second panel shows the adaptive set obtained from farthest points strategy, described in [21]; the third panel shows in blue the geodesics extracted from the adaptive set of points to the root; the fourth panel shows the geodesic density; the fifth panel shows the geodesic density after thresholding.

2.3. Voting with a transport equation

The geodesic voting can be obtained in a different manner without computing the minimal paths. The trajectories y_k computed from (2) are called characteristics for the conservation equation

$$u_t + \mathrm{div}(vu) = 0, \quad (t, x) \in]0, T[\times\Omega, \tag{4}$$

where $v = -\nabla \mathrm{U}$ denotes the velocity field computed from the distance map U. Due to the conservation of the information transported by equation (4) toward the source point, we can define a geodesic density as the integral of the solution of the transport equation (4) in the time T

$$\mu(x) = \int_0^T u(t, x)\mathrm{d}t. \tag{5}$$

The initial conditions in the transport formulation of the geodesic voting determine the set of endpoints used to extract the geodesics in the original formulation of the geodesic voting, presented previously. Here we take as initial condition $u(0, .) = 1$ in the interior of the image domain. A non null

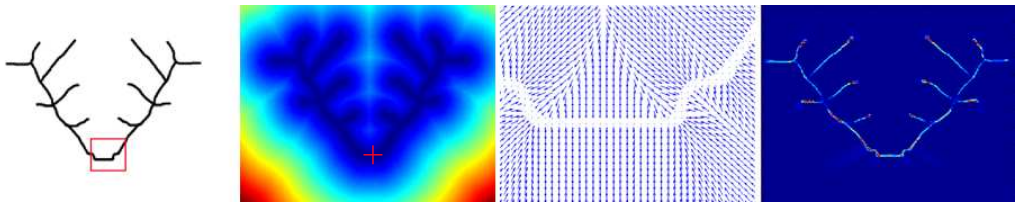

Figure 2: Voting by transport equation. First panel: synthetic image representing a tree structure. Second panel: distance map, the source point is indicated by the red cross. Third panel: zoom on the velocity field shown in the region indicated by the red square in the first panel. Fourth panel: geodesic density computed by relation (6).

value for the initial condition in a given image point means that a geodesic is extracted from this point whereas the value zero means that no geodesic is extracted.

By integration of the transport equation (4) with respect to the time t, we get

$$\mathrm{div}(v\mu) = u(0,x) - u(T,x), \quad x \in \Omega \tag{6}$$

The partial differential equation (6) is not elliptic, so it is more convenient to compute the geodesic density by relation (5) after solving the transport equation (4). Figure 2 shows the segmentation result obtained with this scheme. We have considered a simple synthetic image representing a tree structure like deer woods (see Figure 2-Left). The pixels with high density correspond to the structure extracted from the image (see Figure 2-right).

3. Geodesic voting methods for blood vessel segmentation

Geodesic voting method gives a good approximation of the localization of the tree branches, but it does not allow to extract the tubular aspect of

the tree. Here, we extend the geodesic voting to the segmentation of the boundary of the tubular structure.

3.1. Geodesic voting in an augmented space

In this section we introduce a constraint that ensures that the segmented tree approximates well the centerlines of the tree and we adapt the geodesic voting method to segment the walls of the tubular tree structure. The idea is to perform the geodesic voting with a potential that integrates an extra-dimension used to measure the distance from the centerline to the walls of the vessels. The potential proposed by [24] incorporates this measure. More precisely, this potential is defined by $\tilde{P}:\ (x,r) \in \Omega \times [0,\, r_{max}] \longrightarrow \tilde{P}(x,r)$. It incorporates the full set of image values within the sphere of center x and radii r and it is designed in such a way that the whole sphere lies inside the desired object and is as large as possible so that it is tangential to the boundary of the object. The extension of the minimal path extraction model (1) to the case of a potential with an extra-dimension is achieved by minimizing the following energy

$$\min_{c,r} \int_0^t (\omega + \tilde{P}(c(s), r(s)))\mathrm{d}s. \tag{7}$$

The minimization of this energy allows simultaneous approximation of the minimal path and the radii of the spheres tangents to the boundary of the tube with centers located along the minimal path. The computation of the path is achieved with the framework presented in the Section 2.

Using the potential $\tilde{P}$ and a set of end points (x_k, r_k) (uniform grid) in the domain, we extract a set of geodesics y_k from which we compute the geodesic density $(x,r) \longrightarrow \mu(x,r)$ given by equation (3). In this case the geodesic

voting map is a function of the spatial dimension and also of the radii of the spheres. There are many ways to use this (3D+radius) geodesic density in order to extract the tree structure [22]. Here we use the following spatial density:

$$\tilde{\mu}_m(x) = \sum_{r=0}^{r_{max}} \mu(x, r). \tag{8}$$

Figure 3 illustrates the steps of this method for the segmentation of the tubular aspect of the tree. We can see the efficiency of the method to obtain a segmented tree that is centered in the structure, as well as the precise boundary of the vascular tree.

3.2. Geodesic voting prior to constrain the level set evolution

Here we present a second approach to extract the walls of the vessels using the original geodesic voting method. A shape prior constraint is constructed from the geodesic voting tree to constrain the evolution of a level set active contour in order to extract the walls of the tree. A Bayesian approach is used to introduce this prior into the level set formulation. The model is formulated as a minimization problem of a global energy composed of two terms. The first term corresponds to a deformation energy for a standard region based level set method and the second term introduces the shape prior:

$$E_b(\phi, c_1, c_2) = \mathcal{V}(\phi, c_1, c_2) + \frac{\gamma}{2\sigma^2} \int_\Omega (\phi - \tilde{\phi})^2 \delta_\epsilon(\phi) \mathrm{d}x, \tag{9}$$

where the factor term δ_ϵ allows us to restrict the shape prior within the region of interest, and $\tilde{\phi}$ is the signed distance computed from the geodesic voting tree. The segmentation of vessels with this approach is achieved in two steps:

(1) the geodesic voting tree is extracted using the original geodesic voting method (2) the walls of the vessels are extracted by minimization of the functional E_b. Figure 4 illustrates the segmentation process. Details about this method are given in [23].

3.3. The deformable band

The deformable band method combines aspects of region-based active contours and minimal paths. It is devoted to the recovery of tubular structures. In this context, the segmentation process is constrained by essence, rather than by adding prior shape terms in a general model, see previous section. The band is defined by open curve Γ, parameterized by arc length $s \in [0,1]$, and radius function $\mathcal{R} : [0,1] \rightarrow \mathbb{R}+$. Curve Γ plays the role of the medial axis. The inner region R_{in} of width $2\mathcal{R}$ is bounded by curves $\Gamma_{[\mathcal{R}]}$ and $\Gamma_{[-\mathcal{R}]}$, constructed by translating Γ along normal n.

The band is endowed with energy functional E, weighted sum of the internal energy E_{smooth} and the external region energy E_{data}:

$$E(\Gamma, \mathcal{R}) = \omega E_{smooth}(\Gamma, \mathcal{R}) + (1-\omega) E_{data}(\Gamma, \mathcal{R}) \tag{10}$$

The user-provided coefficient ω, weighting the influence of E_{smooth} over E_{data}, controls the elastic properties of the deformable band. The smoothness energy E_{smooth} is expressed in terms of curve length and radius first order derivative. Since the structure of interest should satisfy an intensity homogeneity criterion, the data term is as follows:

$$E_{data}(\Gamma, \mathcal{R}) = \int_{R_{in}} g_{in}(x)\mathrm{dx} + \int_{\mathrm{R_{out}}} \mathrm{g_{out}(x)dx} \tag{11}$$

where region descriptors g_{in} and g_{out} increase with respect to intensity inhomogeneity. The initial curve Γ is built using the geodesic voting method.

The deformable band approach, described above, was extended to 3D in [25]. In this section we show the feasibility of the geodesic voting method in 3D.

Figures 5 and 6 depict results obtained with the 3D tree method applied on a CT volume data. Figure 6-right represents a slice of the CT data, with centerlines and surface positions of two segments (aorta and superior mesenteric artery). With a C++ implementation running on an Intel Core 2 Duo 2.2GHz PC (4Gb RAM), computational costs for a $256 \times 256 \times 256$ volume image is 28s for extractiong the surface, see the result in Figure 5. According to visual inspection, we believe the reconstruction results to be promising.

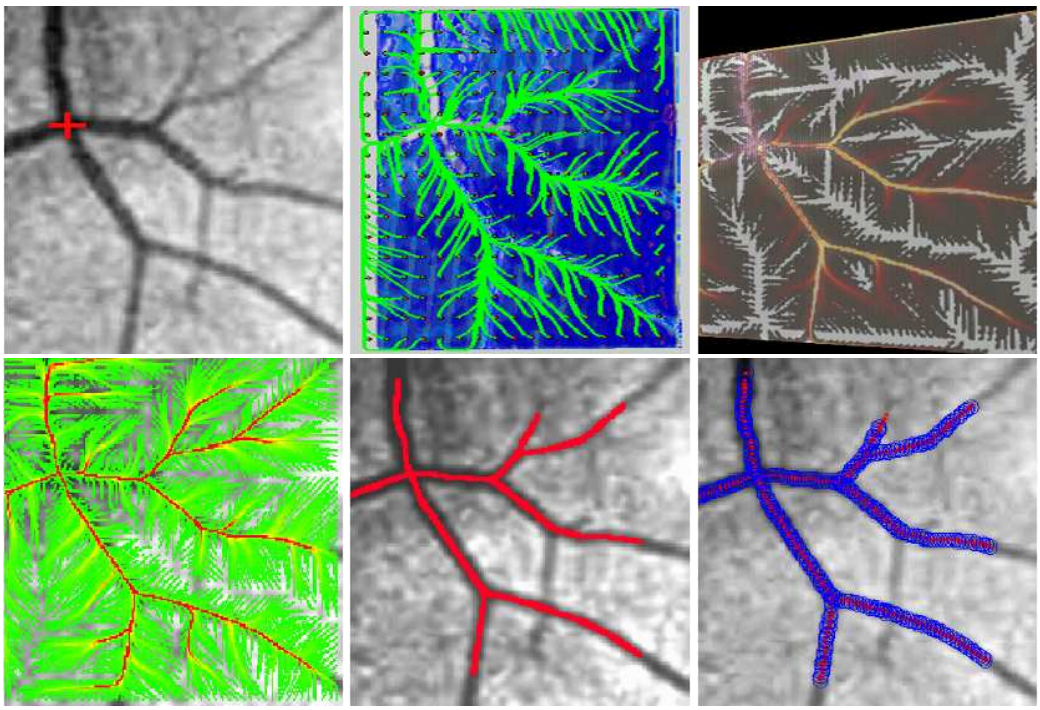

Figure 3: Vessel segmentation from a 2D retinal image with the geodesic voting method. First row: the left shows a 2D retinal image, the red cross indicates the source point; the center panel shows, in (2D+radius) domain, in green the paths extracted from a uniform grid to the source point; the right panel shows the density computed in (2D+radius) domain, yellow color corresponds to high density and brown to low density. Second row: the left panel shows the geodesic density $\tilde{\mu}_m$, given by equation (8), red color corresponds to high density, yellow color to medium, and green color to low density; the center panel shows in red the density $\tilde{\mu}_m$ after thresholding; the right panel shows in blue the extraction result of the tubular structure obtained by thresholding the map $\{\tilde{\mu}_m, \tilde{r}\}$, where $\tilde{r}(x) = \arg \max_{r \in [0, r_{max}]} \tilde{\mu}_m(x, r)$.

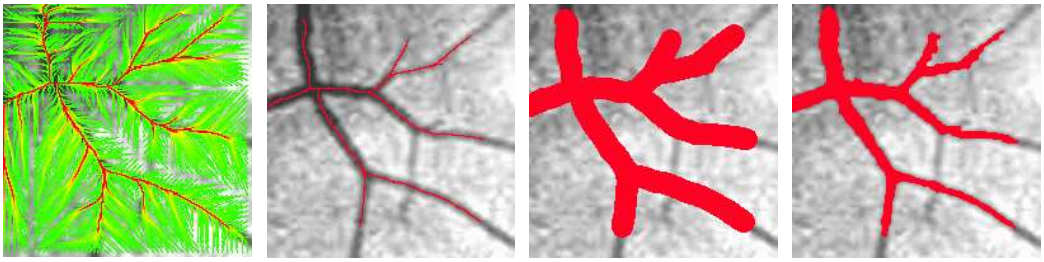

Figure 4: Geodesic voting segmentation of vessels from a 2D retinal image. From left to right: adaptive voting on the image; voting tree obtained by thresholding the geodesic voting; shape prior obtained by dilation of the voting tree; segmentation result obtained with region based active contour with prior (method described in Section 3.2).

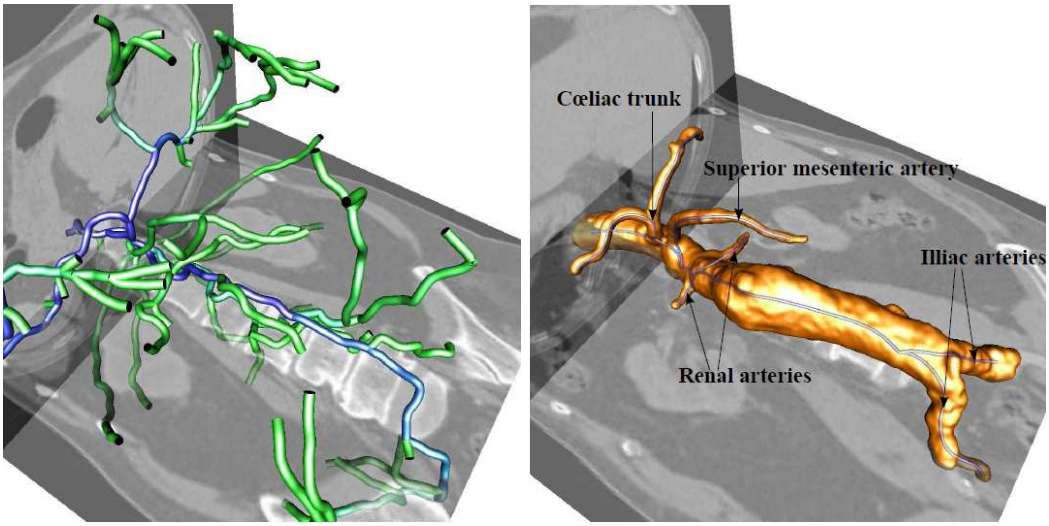

Figure 5: Tree after thresholding on voting score (left) and final tree with boundary surface (right)

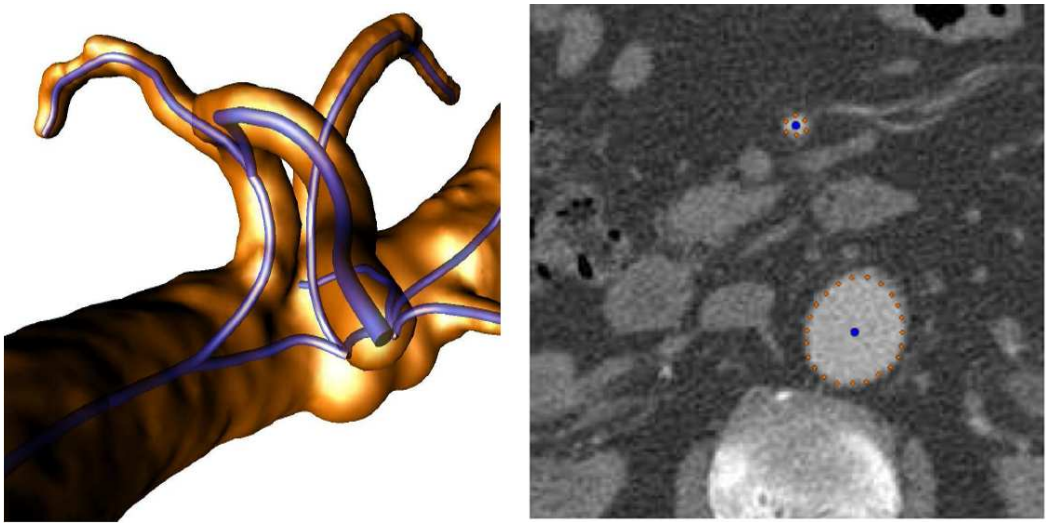

Figure 6: A close look at the boundary surface. Left panel: a representation with centerlines; right panel: Slice of the 3D CT image, with centerlines and surface positions of two segments: aorta (bottom) and superior mesenteric artery (top)

4. Results and discussion

In this section, we will compare GVR (method with radius presented in Section 3.1) and GVP (method with prior presented in Section 3.2) with other approaches (the edge based level set method [26], the Chan and Vese method [27], and the fuzzy connectedness method [28]) for vessel segmentation from retinal images on the DRIVE data (Digital Retinal Images for Vessel Extraction) [29].

The DRIVE data were acquired using a Canon CR5 non-mydriatic 3CCD camera with a 45 degree field of view (FOV). Each image was captured using 8 bits per color plane at 768 by 584 pixels. The FOV of each image is circular with a diameter of approximately 540 pixels. For this database, the images have been cropped around the FOV. The DRIVE data is composed of 40 images from different subjects for which manual segmentations are also provided.

Considering the complexity of the retinal images and the properties of our algorithm, we have cropped twelve different images from the 40 images available and evaluated our method on them. Note that the retinal vessels in each image do not correspond to a tree structure. Some images may contain several disconnected trees or networks. Note that when the image contains more than one tree structure, the geodesic voting method tends to create connections between them. These connections may not make sense anatomically, therefore a preprocessing or postprocessing step is necessary to get an accurate segmentation. For a completely automated application, this problem may be solved by using the selection step proposed (for a different method) in [30] to remove paths that are unlikely to belong to the microglia

extensions. This is out of focus of this paper to propose precise automatic pre- or post-processing to deal with all kind of situations. Therefore, it was more illustrative to choose images that contain tree structures and then crop the image in such way that the cropped image contains only one tree structure. We were able to extract 12 tree structures from 12 different images in the DRIVE data. The size of the cropped image depends on the size of the tree in the original image and in average corresponds to 100 pixels in high and 50 pixels in width.

For the GVR method, the augmented potential $\tilde{P}$ used is described in Section 3.1. The starting point was chosen as a junction of the tree. As the end points were chosen as a uniform grid, the spatial starting point can be chosen anywhere within the tree. However, the starting radii should be chosen carefully to get an optimal segmentation. In our experiments on DRIVE data we obtained good estimation of these parameters by testing different values following the study presented in [24]. These parameters can be optimized and automated for a given class of images.

For the GVP method, we have used the following potential $P(x) = I(x)^3$ to run the geodesic voting segmentation, where I is the grayscale intensity of the image. The value of γ, the weight on the prior, was chosen empirically and used for all the experiments presented in the paper. We showed in [31] that this value can be chosen in a large range with the same efficiency.

In figures 7 and 8 (results obtained with the GVR and GVP), the source point used to perform the geodesic voting was chosen empirically on the junction of the tree that is connected to the largest number of branches. This allows us to segment the largest number of branches in the presence

of small branches with weak contrast. Note that the quality of the images provided by DRIVE are not very good and sometimes it is hard to set optimal sphere radii for the GVR initialization. When it is not possible to give a precise radius we underestimate the value of the radius whenever possible, indeed we measure the radii of the spheres in pixels and their diameters are odd numbers. Concerning the end points, we have used the same number for each method: 1200 farthest points (generated by the process described in [21]) for the GVP method, and a uniform grid of the augmented potential for the GVR method. The threshold for the geodesic density was defined from the first five images as the mean value of all the threshold values manually selected for these five image. Then this mean threshold was used for all the twelve images. We have used two different values for the mean threshold: one value for the GVP method and the other for the GVR method.

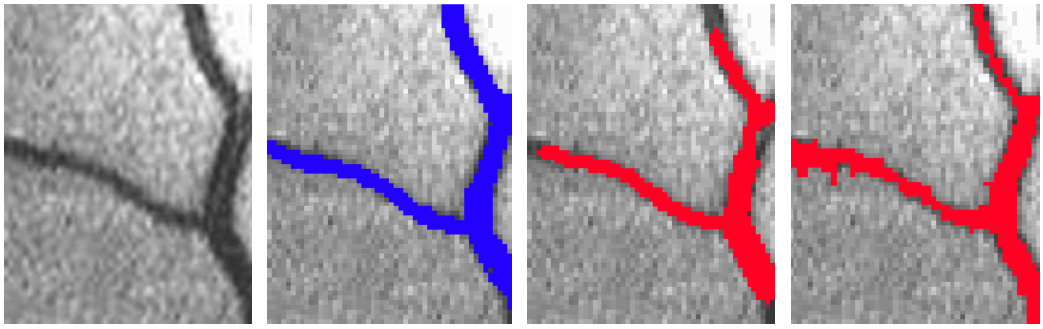

Figure 7: Blood vessels segmentation using the GVR and GVP methods from one of the twelve cropped retinal images (DRIVE data). The left panel shows the original image; the second panel shows in blue the manual segmentation; the third panel shows the segmentation result obtained with the GVR method; the right panel shows the segmentation result obtained with the GVP method.

In [32], we compare the GVR and GVP results for vessel segmentation

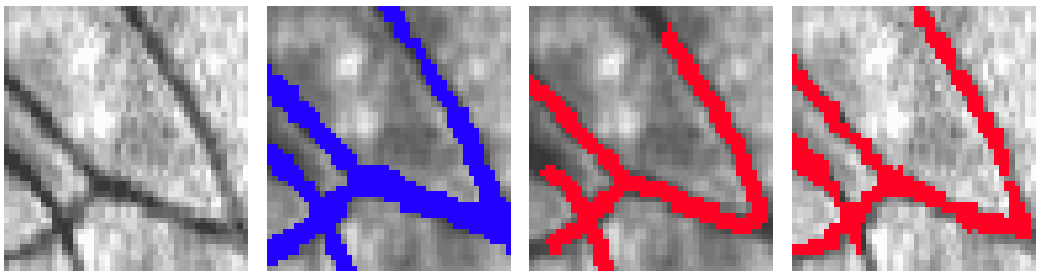

Figure 8: Blood vessels segmentation using the GVR and GVP methods from one of the twelve cropped retinal images (DRIVE data). The left panel shows the initial image; the second panel shows in blue the manual segmentation; the third panel shows in red the segmentation obtained with GVR method; the right panel shows the segmentation obtained with our GVP method.

on the DRIVE database in terms of the following evaluation measures: Dice, specificity, and sensitivity. We found that the GVR and GVP gave similar results.

In the sequel, we compare the performance of GVR and GVP methods with the edge and region based level set methods and the fuzzy connectedness method in the segmentation of vessels.

Figure 9 shows the results obtained with the fuzzy connectedness method [28]. The segmentation of the tree is obtained by thresholding the fuzzy connectedness map. For a small threshold the method does not allow to extract all the branches of the tree, and when the threshold is increased the propagation leaks outside of the tree. The same problems were observed with the edge based level set method [26] when we increased the number of iterations, see Figure 10. The shape prior allows us to constrain the propagation inside the tubular tree. Figure 11 shows that the propagation without shape constraints ($\gamma = 0$ in equation (9)) can leak outside of the

tree structure.

Our methods (GVP and GVR) give the best results: they succeed in segmenting more tree branches without leaking outside of the tree structures.

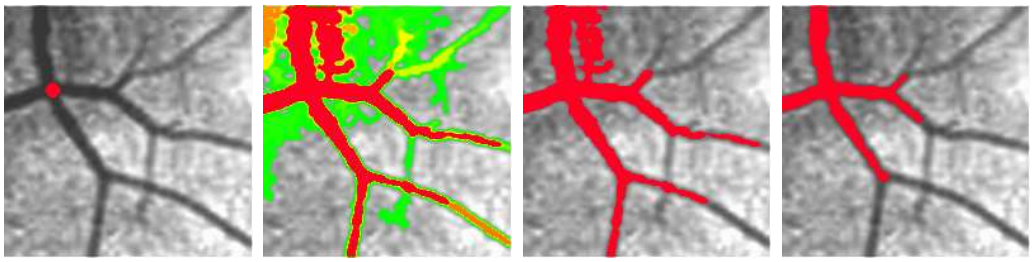

Figure 9: Fuzzy connectedness segmentation. The panels show from the left to the right: the localization of the red seed point; the fuzzy connectedness map; the thresholded fuzzy connectedness map with the threshold set at th_1 (third panel); the thresholded fuzzy connectedness map with a threshold set at th_2 superior to th_1.

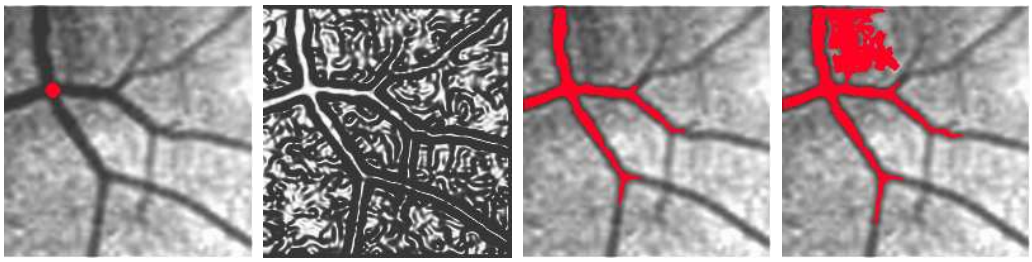

Figure 10: Edge based Level set method. The left panel shows in red the initial position of the interface; second panel shows the sigmoid of the gradient magnitude; the third panel shows the interface after 1000 iterations; the right panel shows the interface after 2000 iterations.

5. Conclusion

In this paper we have presented a completely new approach for the segmentation of tree structures based on geodesic voting. This approach is

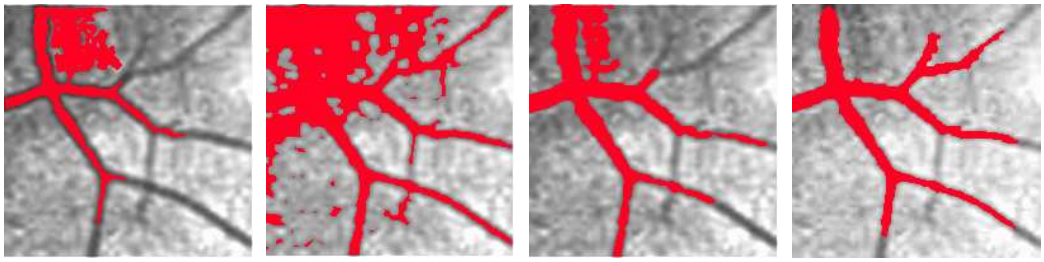

Figure 11: Comparison of the geodesic voting approach (GVP) with other methods. The left panel shows in red the segmentation obtained by edge based level set method; the second panel shows in red the segmentation results obtained with a Chan and Vese method without using the geodesic voting prior; the third panel shows the fuzzy connectedness segmentation; the right panel shows the segmentation result obtained with our geodesic voting with prior (GVP).

adapted to automatically segment tree structures from a single point provided by the user with no further a priori information required about the tree. By contrast, other methods described in the literature for the segmentation of tree structures are not fully automatic and require prior information about the tree to be segmented. We have combined this approach with an added fourth dimension (space+radius) or with region-based level sets using priors in order to obtain both the centerlines and boundaries of the tree. We have applied our geodesic voting approach to segment different tree structures from a variety of bio-medical images. Finally, we have evaluated our approach on retinal 2D images, and have shown segmentation results on 3D data. The results were satisfying and promising.

Acknowledgments

The authors would like to thank Julien Mille for his collaboration to combine the geodesic voting and the deformable band methods.

References

[1] C. Kirbas, F. Quek, A review of vessel extraction techniques and algorithms, ACM Comput. Surv. 36 (2) (2004) 81–121.

[2] D. Lesage, E. D. Angelini, I. Bloch, G. Funka-Lea, A review of 3D vessel lumen segmentation techniques: Models, features and extraction schemes, Medical image analysis 13 (6) (2009) 819–845.

[3] K. Mori, J. Hasegawa, J. Toriwaki, H. Anno, K. Katada, Recognition of bronchus in three-dimensional X-ray CT images with application to virtualized bronchoscopy system, Pattern Recognition, International Conference on 3 (1996) 528–532.

[4] G. Agam, S. G. Armato III, C. Wu, Vessel tree reconstruction in thoracic CT scans with application to nodule detection, IEEE Trans. Med. Imaging 24 (4) (2005) 486–499.

[5] J. Carrillo, M. Hernández Hoyos, E. Davila-Serrano, M. Orkisz, Recursive tracking of vascular tree axes in 3D medical images, Int J Comput Assisted Radiol Surg 1 (6) (2007) 331–339.

[6] P. Lo, J. Sporring, H. Ashraf, J. J. H. Pedersen, M. de Bruijne, Vessel-guided airway tree segmentation: A voxel classification approach, Medical Image Analysis 14 (4) (2010) 527–538.

[7] L. Lorigo, O. Faugeras, W. Grimson, R. Keriven, R. Kikinis, A. Nabavi, C.-F. Westin, Curves: Curve evolution for vessel segmentation, Medical Image Analysis 5 (2001) 195–206.

[8] R. D. Swift, A. P. Kiraly, A. J. Sherbondy, A. L. Austin, E. A. Hoffman, G. McLennan, W. E. Higgins, Automatic axis generation for virtual bronchoscopic assessment of major airway obstructions, Computerized Medical Imaging and Graphics 26 (2) (2002) 103 – 118.

[9] S. Bouix, K. Siddiqi, A. Tannenbaum, Flux driven automatic centerline extraction, Medical Image Analysis 9 (3) (2005) 209–221.

[10] A. F. Frangi, W. J. Niessen, R. M. Hoogeveen, T. van Walsum, M. A. Viergever, Model-based quantitation of 3D magnetic resonance angiographic images, IEEE Trans. Med. Imaging 18 (10) (1999) 946–956.

[11] R. Manniesing, B. K. Velthuis, M. S. van Leeuwen, I. C. van der Schaaf, P. J. van Laar, W. J. Niessen, Level set based cerebral vasculature segmentation and diameter quantification in CT angiography, Medical Image Analysis 10 (2) (2006) 200–214.

[12] P. Yan, A. A. Kassim, Segmentation of volumetric MRA images by using capillary active contour, Medical Image Analysis 10 (3) (2006) 317–329.

[13] T. Deschamps, L. D. Cohen, Minimal paths in 3D images and application to virtual endoscopy, in: Sixth European Conference on Computer Vision, Dublin, Ireland, ECCV(2), 2000, pp. 543–557.

[14] O. Wink, W. J. Niessen, B. Verdonck, M. A. Viergever, Vessel axis determination using wave front propagation analysis, in: MICCAI '01: Proceedings of the 4th International Conference on Medical Image Computing and Computer-Assisted Intervention, Springer-Verlag, London, UK, 2001, pp. 845–853.

[15] T. Deschamps, L. D. Cohen, Fast extraction of minimal paths in 3D images and applications to virtual endoscopy, Medical Image Analysis 5 (4) (2001) 281 – 299.

[16] L. D. Cohen, T. Deschamps, Multiple contour finding and perceptual grouping as a set of energy minimizing paths, in: Proc. of Third International Conference on Energy Minimization Methods in Computer Vision and Pattern Recognition (EMMCVPR - 2001), Springer Lecture Notes in Computer Science 2134, Sophia-Antipolis, 2001, pp. 560–575.

[17] L. D. Cohen, R. Kimmel, Global minimum for active contour models: A minimal path approach, International Journal of Computer Vision 24 (1) (1997) 57–78.

[18] M. A. Gülsün, H. Tek, Robust vessel tree modeling, in: MICCAI (1), New York, NY, 2008, pp. 602–611.

[19] L. D. Cohen, T. Deschamps, Segmentation of 3D tubular objects with adaptive front propagation and minimal tree extraction for 3D medical imaging, Math. Models Methods Appl. Sci. 10 (4) (2007) 289–305.

[20] Y. Rouchdy, L. D. Cohen, Image segmentation by geodesic voting. application to the extraction of tree structures from confocal microscope images, in: The 19th International Conference on Pattern Recognition, Tampa, Florida, 2008, pp. 1–5.

[21] Y. Rouchdy, L. D. Cohen, The shading zone problem in geodesic voting and its solutions for the segmentation of tree structures. application to the segmentation of microglia extensions, in: MMBIA 2009: IEEE

Computer Society Workshop on Mathematical Methods in Biomedical Image Analysis in conjunction with CVPR'09, Miami, Florida, USA, 2009, pp. 66–71.

[22] Y. Rouchdy, L. D. Cohen, A geodesic voting method for the segmentation of tubular tree and centerlines, in: Eigth IEEE International Symposium on Biomedical Imaging (ISBI'11), Chicago, Illinois, USA, 2011, pp. 979–983.

[23] Y. Rouchdy, L. D. Cohen, A geodesic voting shape prior to constrain the level set evolution for the segmentation of tubular trees., in: Third International Conference on Scale Space and Variational Methods in Computer Vision (SSVM), Ein-Gedi, Israel, 2011, pp. 1–12.

[24] H. Li, A. Yezzi, Vessels as 4D curves: Global minimal 4D paths to extract 3D tubular surfaces and centerlines, IEEE Transactions on Medical Imaging 26 (2007) 1213–1223.

[25] J. Mille, L. Cohen, Deformable tree models for 2D and 3D branching structures extraction, Computer Vision and Pattern Recognition Workshop on Mathematical Methods in Biomedical Image Analysis (MMBIA) 0 (2009) 149–156.

[26] R. Malladi, J. A. Sethian, B. C. Vemuri, Shape modeling with front propagation: A level set approach, IEEE Trans. Pattern Anal. Mach. Intell. 17 (2) (1995) 158–175.

[27] T. F. Chan, L. A. Vese, Active contours without edges, IEEE Trans. Med. Imaging 10 (2) (2001) 266 –277.

[28] J. K. Udupa, P. K. Saha, R. de Alencar Lotufo, Relative fuzzy connectedness and object definition: Theory, algorithms, and applications in image segmentation, IEEE Trans. Pattern Anal. Mach. Intell. 24 (11) (2002) 1485–1500.

[29] J. Staal, M. Abramoff, M. Niemeijer, M. Viergever, B. van Ginneken, Ridge based vessel segmentation in color images of the retina, IEEE Trans. Med. Imaging 23 (4) (2004) 501–509.

[30] Y. Rouchdy, L. D. Cohen, O. Pascual, A. Bessis, Minimal path techniques for automatic extraction of microglia extensions, International Journal for Computational Vision and Biomechanics 4 (1) (2011) 35–42.

[31] Y. Rouchdy, I. Bloch, A chance-constrained programming level set method for longitudinal segmentation of lung tumors in CT, in: Conf Proc IEEE Eng Med Biol Soc., 2011, pp. 3407–10.

[32] Y. Rouchdy, L. D. Cohen, Retinal blood vessel segmentation using geodesic voting methods, in: 9th IEEE International Symposium on Biomedical Imaging: From Nano to Macro, ISBI 2012, May 2-5, 2012, Barcelona, Spain, Proceedings, 2012, pp. 744–747.